

Spectroscopy of highly excited vibrational states of HCN in its ground electronic state

R. Z. Martínez^{a)} and Kevin K. Lehmann

Chemistry Department, Princeton University, Princeton, New Jersey 08544

Stuart Carter

Department of Chemistry, University of Reading, Reading RG6 2AD, United Kingdom

(Received 21 July 2003; accepted 14 October 2003)

An experimental technique based on a scheme of vibrationally mediated photodissociation has been developed and applied to the spectroscopic study of highly excited vibrational states in HCN, with energies between 29 000 and 30 000 cm^{-1} . The technique consists of four sequential steps: in the first one, a high power laser is used to vibrationally excite the sample to an intermediate state, typically (0,0,4), the ν_3 mode being approximately equivalent to the C–H stretching vibration. Then a second laser is used to search for transitions between this intermediate state and highly vibrationally excited states. When one of these transitions is found, HCN molecules are transferred to a highly excited vibrational state. Third, a ultraviolet laser photodissociates the highly excited molecules to produce H and CN radicals in its $A^2\Pi$ electronic state. Finally, a fourth laser (probe) detects the presence of the CN(A) photofragments by means of an $A \rightarrow B \rightarrow X$ laser induced fluorescence scheme. The spectra obtained with this technique, consisting of several rotationally resolved vibrational bands, have been analyzed. The positions and rotational parameters of the states observed are presented and compared with the results of a state-of-the-art variational calculation.

© 2004 American Institute of Physics. [DOI: 10.1063/1.1631253]

I. INTRODUCTION

The molecule of HCN has been, through the years, the subject of numerous theoretical and experimental studies. The reasons for this interest are multiple: from the theoretical point of view, a small, linear polyatomic molecule is an ideal candidate for the development and testing of models aimed to calculate and reproduce its structure of rotational, vibrational, and electronic states, as well as its geometry and related molecular properties. HCN presents the additional interest of being a highly anharmonic species, which has allowed probing a wide range of vibrational states. Moreover, the possibility of intramolecular isomerization $\text{HCN} \leftrightarrow \text{HNC}$ has also made this a favorite model system for the study of unimolecular reactions. From a more applied point of view, the interest in HCN has also raised in the last decades among astrophysicists due to the detection of its presence in the atmospheres of carbon stars: numerous diffuse absorptions in the spectra of light coming from these stars have been identified as produced by hot band transitions in HCN.¹

Early spectroscopic studies of HCN consisted mainly of absorption spectra in the medium infrared (IR) region. The first IR spectrum, in which the frequency of the C–H stretch fundamental vibration was measured, was recorded as early as 1913.² In subsequent years, and using similar techniques, a number of experiments were performed that allowed a more precise determination of the frequencies of the funda-

mental vibrations and the observation of new, more excited vibrational states, although with relatively low resolutions.^{3–8} States up to (0,0,5),⁹ with an energy of $\sim 15\,552 \text{ cm}^{-1}$, had been observed by 1945, as summarized by Herzberg.¹⁰ Also, some UV absorption studies were carried out during this period that revealed a complex structure of electronic states.^{11–14}

Work on the IR and microwave region of the spectrum continued in subsequent years, mainly through the use of absorption measurements. Douglas and Sharma¹⁵ used very long absorption paths and photographic recording to observe for the first time the (0,0,6) state, which lies at $\sim 18\,377 \text{ cm}^{-1}$. A number of other authors obtained spectra that improved considerably the quality of the available vibrational and rotational constants for the ground and excited vibrational states.^{16–23} The line intensity measurements also obtained in some of these works allowed a comparison with the results of theoretical papers^{24–26} dealing with the calculation of bond dipoles and dipole moment derivatives. More detailed theoretical calculations, involving the construction of potential energy surfaces and their fitting to experimental data, were also carried out by a number of authors.^{27–29}

As the capabilities of experimental techniques improved over the years, so did the quality of the data obtained: very high resolution measurements on HCN were performed with an intracavity photoacoustic technique in 1982,³⁰ covering the region between 15 000 and 18 500 cm^{-1} . The low and medium energy region of the potential was further explored in later years by different groups using diverse experimental techniques like stimulated emission pumping (SEP), Fourier-transform infrared (FTIR) and laser diode absorption spectroscopy,^{31–37} all of which yielded a large volume of

^{a)}Present address: Physical Chemistry Lab, Chemistry Department, University of Helsinki, FIN-00014, Finland. Electronic mail: raul.martinez@helsinki.fi

high-quality data. This availability of accurate experimental data on vibrationally excited states also encouraged the refinement of the theoretical calculations and the development of better potential energy surfaces.^{38–42} In more recent years new experimental contributions have been made, including the observation of new excited states in HCN and various of its isotopomers^{43–51} and collisional relaxation measurements.^{52,53} The highest vibrational level experimentally observed in HCN lies at $\sim 23\,000\text{ cm}^{-1}$, corresponding to the (1,1,7) state. Its observation⁴³ was made possible through the use of a very sensitive detection scheme, cavity ring-down spectroscopy.

As mentioned before, the possibility of $\text{HCN} \leftrightarrow \text{HNC}$ unimolecular isomerization has also attracted the attention of numerous authors: although there were some previous spectral studies of HNC isolated in low-temperature matrices,^{54,55} this species was experimentally observed for the first time in gas phase by radioastronomers in interstellar space in 1971.^{56,57} The amount of HNC in equilibrium with HCN is almost negligible at room temperature,⁵⁸ and it was not until a procedure for synthesizing HNC in a flowing afterglow of nitrogen was developed⁵⁹ that gas-phase measurements could be made and the first IR and microwave spectra were obtained in a laboratory. Variations of this same procedure have been used in a number of experiments.^{59–66} An alternative approach used by Maki and Sams⁵⁸ consists of working at temperatures close to 1000 K to shift the $\text{HCN} \leftrightarrow \text{HNC}$ equilibrium towards HNC and reach a concentration of this species high enough as to allow the recording of absorption spectra in a static sample. More recently, Northrup and co-workers used time-resolved IR absorption spectroscopy to probe HNC molecules generated by collisions of translationally hot H atoms with halogen cyanides.⁶⁷ All these experiments have produced a wealth of data that, combined with the results of the many theoretical works also devoted to the subject (see, for example, Refs. 68–77), provides a reasonably accurate picture of the vibrational and rotational structure of HNC and sheds some light on the problem of unimolecular isomerization in the HCN–HNC system: the ground state of HNC lies $\sim 4900\text{ cm}^{-1}$ above the ground state of HCN, with the two minima of the potential energy surface separated by an isomerization barrier that has been calculated to be of $\sim 15\,400\text{ cm}^{-1}$.⁷³ This means that, although with an excitation of only two quanta in the C–H stretch of HCN the isomerization would be energetically possible, the need to tunnel through the barrier makes it quite unlikely. The picture suggests, however, the very attractive possibility of studying the isomerization through spectroscopy of very excited vibrational states of HCN: theoretically, it could be possible to detect this reaction by looking at perturbations in the spectra of vibrationally excited states of HCN located above the barrier (or, in other words, observe states that are delocalized over the two minima of the $\text{HCN} \leftrightarrow \text{HNC}$ potential energy surface). According to calculations, the reaction coordinate for the isomerization has a strong bend character,^{68,72} but so far no positive spectroscopic evidence of this isomerization has been found by the authors that have probed the energy region of the HCN surface above the barrier. Wodtke and co-workers³⁶ used SEP to explore a region

of the potential energy surface up to $18\,900\text{ cm}^{-1}$ and observe highly excited bending modes, but no delocalized states were found. For the highest energy states that have been studied up to the present date, more than 7000 cm^{-1} above the barrier,⁴³ little mixing was found between the stretching and bending states, and thus no evidence of unimolecular isomerization. However, experimental measurements of thermal dissociation of HCN⁷⁸ show dissociation rates that are close to those predicted by the Rice–Ramsperger–Kassel–Marcus (RRKM) theory, which implies that a strong mixing of all the vibrational modes must occur as one approaches the dissociation limit. So far, clear evidence of this mixing has not been observed in states studied spectroscopically.

The purpose of the present work is to extend the range of studied vibrational states in the ground electronic state of HCN by exploring the region of the potential energy surface near $30\,000\text{ cm}^{-1}$ and accurately determine the positions of the vibrational states present in this region. The interests of this kind of measurement are multiple: first, it provides new experimental data involving a potential energy surface that, although well known at lower energy values, is unstudied in this highly excited region. This will allow a comparison with the data resulting from state-of-the-art theoretical calculations. Second, and following from the discussion above, it is of great interest to search for evidence of mode mixing and perhaps unimolecular isomerization in this high-energy region of the potential energy surface: since it lies $\sim 7000\text{ cm}^{-1}$ above the highest state previously studied these effects are more likely to be observed here. Additionally, in this region the CN and CH stretching vibrations should tune into nearly 1-1 resonance, which could lead to qualitative changes in the spectrum and even classical chaos due to overlapping resonances given the fact that the 3-2 resonance is also known to be of importance starting with the (0,0,4)-(3,0,2) resonance pair. Finally, the spectra also provide information about processes of intramolecular vibrational relaxation (IVR) that may take place between the highly excited states present in this region. It must be noted that the experimental setup chosen for our study is based on the technique of vibrationally mediated photodissociation (VMP) introduced by Crim.⁷⁹ This technique has already been used in our laboratory to study the photodissociation of HCN^{80,81} vibrationally excited to its (0,0,4) state. It is our purpose to continue developing the same line of work and adapt the experimental configuration we describe in this paper to the study of IVR processes in this energy region near $30\,000\text{ cm}^{-1}$, where strong interactions can be expected due to the higher energy and higher density of states. The experimental approach used in this work is similar to that independently used by Barnes, Gross, and Sinha to study vibrational states of H_2O in the $22\,000\text{--}25\,000\text{ cm}^{-1}$ wavenumber region.⁸²

II. EXPERIMENT

Figure 1 shows a simplified representation of the four-step process used in this work to obtain spectra of highly excited vibrational states of HCN. In the first two steps (that from now on will be referred to as “pump” and “jump”), two laser pulses are used to sequentially excite HCN,

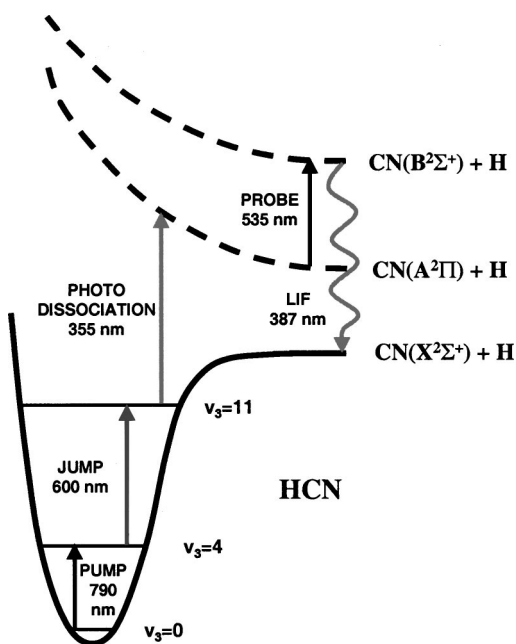


FIG. 1. Overview of the four-step spectroscopic technique.

through an intermediate vibrational state, to a highly excited vibrational state in the energy region around $30\,000\text{ cm}^{-1}$ ($v_3 = 11$ in our example). Within nanoseconds of this double excitation a third laser pulse photodissociates the highly excited HCN, rendering as main products the radicals H and CN($A^2\Pi$). Finally, after a delay to allow thermalization, a fourth laser pulse (“probe”) is used to detect the presence of these CN(A) photofragments by means of laser induced fluorescence (LIF) using the $A \rightarrow B^2\Sigma^+ \rightarrow X^2\Sigma^+$ excitation and spontaneous emission sequence.

Of the four laser pulses involved in the experiment, only the frequency of the jump laser, used for the second vibrational excitation, is scanned during the experiments reported below. The frequencies of the pump and probe lasers are tuned to well-known transitions of HCN and CN, respectively, and remain fixed during the experiment, and the frequency of the photodissociation laser is also kept constant at a value that provides enough energy for this photodissociation to take place when HCN molecules are vibrationally excited to the $30\,000\text{ cm}^{-1}$ region. In this way, every time the frequency of the jump photon matches that of a transition between the intermediate vibrational state and a highly excited vibrational state in the above mentioned region, CN(A) photofragments are produced and electronically excited and a fluorescent emission detected. This allows us to obtain, by scanning the jump frequency, a rovibrational spectrum that shows the transitions between the intermediate and the highly excited vibrational states.

The first photon of the sequence (pump) is used to excite the HCN sample from the ground vibrational state to an intermediate excited vibrational state, that in all our experiments has been the (0,0,4). The choice of this particular state represents a compromise between the efficiency of the first and the second vibrational excitations: lower vibrational states are easier to populate from the ground state, but the efficiency of the population transfer from these intermediate

to the final states is then very poor. The use of higher intermediate vibrational states presents the opposite problem, with the efficiency of the population transfer from the ground to the intermediate state becoming too small.

The second excitation photon (jump) illuminates the HCN sample several nanoseconds after the first photon has excited it, and its frequency is scanned to search for rovibrational transitions from the now populated (0,0,4) state to highly excited states. When the frequency of the jump photon matches the frequency of one of these transitions an effective population transfer takes place. The high anharmonicity of HCN plays a key role in the efficiency of this process: According to our calculations,⁸³ the absorption cross section for a transition from the (0,0,4) intermediate state to a highly excited state like (2,0,9), with a change of seven quanta of vibrational excitation, is of the same order as the absorption cross section for the transition from the ground to the (0,0,4) state, with a change of only four quanta. This result is a consequence of the potential energy surface being very anharmonic in the C–H stretching coordinate. Since the intensity of overtone transitions comes mainly from the anharmonic terms of the potential,⁸⁴ a transition involving two excited states, one of them highly excited, benefits from a greater contribution from the anharmonic parts of the wave functions of these states than a transition involving one excited state and the ground state, this last one having a relatively small anharmonic part in its wave function. This effect is essential in our experiment, since it allows us to populate highly excited states that would otherwise be very difficult to reach. On the other hand, the applicability of our experimental scheme is somewhat limited to molecules showing this highly anharmonic behavior, of which the light hydrides (HCN, H₂O, H₂S) are one of the best examples. The enhancement of the overtone transition further requires that there be no or limited IVR in the intermediate state, since that will dilute the excited X–H bond character of the eigenstates and lead to reduction of the cross section for the jump transition.

The third photon of the sequence is used to photodissociate the HCN molecules that have reached the highly excited vibrational states and produce the H and CN(A) radicals. The energy of the photon needs to be high enough to photodissociate HCN molecules from a highly excited vibrational state, but not enough to photodissociate those in the ground or in the (0,0,4) excited state. In this way, only when some HCN molecules reach the highly excited states we want to study an effective production of CN(A) radicals takes place.

Finally, the fourth photon of the sequence (probe) is used to detect the presence of CN(A) radicals by probing the electronic transition between its A and B excited electronic states, both of which are spectroscopically well known (see, for example, Refs. 85–87). The CN(B) radical shows a very strong fluorescent emission to the ground electronic state X with a lifetime of about 60 ns,⁸⁸ that can be easily detected with a photomultiplier. The reason that the LIF detection scheme was adopted instead of a simpler $A \rightarrow X$ spontaneous emission scheme was that in a previous VMP study⁸⁰ of the (0,0,4) state, $A \rightarrow X$ emission was not detected despite the

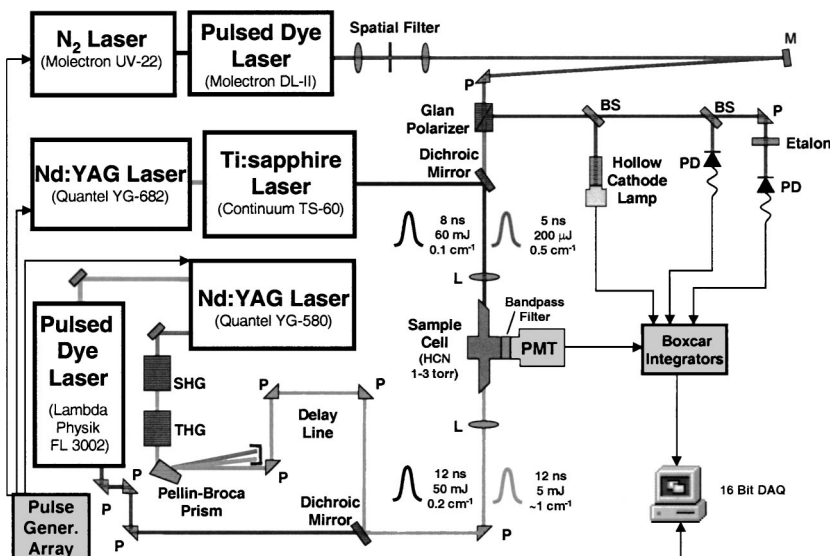


FIG. 2. Schematic of the experimental setup.

fact that LIF later proved that $CN(A)$ was the primary dissociation product. The reason for this failure was likely due to the long radiative lifetime of the A state,⁸⁸ plus the fact that its emission is in the near IR. The cooled Ge detector used to detect the $A \rightarrow X$ emission had a noise equivalent power orders of magnitude higher than the photomultiplier used to detect the $B \rightarrow X$ emission.

Figure 2 shows a schematic of the experimental setup. Three synchronized laser systems are used to sequentially generate the four light pulses required for the experiment. These pulses are focused into a cell containing the HCN sample, where a 90° mounted photomultiplier is used to detect the fluorescent emission of the excited $CN(B)$ photofragments. The output signal of the photomultiplier tube (PMT) is then sent to a gated integrator and from there to a PC computer for storage and analysis.

The first pulse of the sequence is generated in a Ti:sapphire laser (Continuum NY61) pumped by the second harmonic of a pulsed Nd:YAG laser (Quantel YG682) with a repetition rate of 10 Hz. Typical values for the pulse energy and duration are 60 mJ and 8 ns full width at half maximum (FWHM). The spectral width is of about 0.1 cm^{-1} , which allows population transfer to the $(0,0,4)$ state through a single rotational transition and thus excitation of a single rotational state of our choice. The transition used in most of our experiments has been the $R(8)$ and, in some of them, the $R(12)$, with wavenumbers of $12\,658.6$ and $12\,666.3 \text{ cm}^{-1}$, respectively. The high energy output of the laser allows, when combined with tight focusing conditions, saturation or near-saturation of these transitions. A 360 mm focal length lens was used to focus the beam into the sample cell. Fine tuning of the laser frequency was achieved by sending a small fraction of the beam to an auxiliary photoacoustic cell—not displayed in Fig. 2 for the sake of simplicity—filled with 50 Torr of HCN and maximizing the photoacoustic signal.

The jump pulse is generated by a dye laser (Lambda Physik FL3002) pumped by the second harmonic of a Nd:YAG laser (Quantel YG580-10 upgraded with an amplifier), and has energies between 50 and 60 mJ depending on

the dye being used. Rhodamine 610, Rhodamine 590, and Fluorescein 27 were used in our experiments, allowing us to explore the wavelength region between 620 and 550 nm. The duration of the pulses is 12 ns FWHM and the linewidth is of about 0.2 cm^{-1} , again narrow enough to allow excitation of a single rotational transition between the $(0,0,4)$ and the highly excited state. The beam is focused into the sample cell—in counterpropagation with respect to the pump beam—by a 450 mm focal length UV-silica lens. After emerging from the cell, three fractions of the beam are taken and sent to a photodiode, a hollow cathode lamp and a reference etalon to monitor its power, frequency, and the linearity of the scan.

The photodissociation pulse is generated by the same Nd:YAG laser that pumps the Lambda Physik dye laser: the fraction of the Nd:YAG laser beam that remains at the fundamental wavelength after the second harmonic generation process used to pump the dye laser is sent through another second harmonic generator and then a third harmonic generator, producing laser pulses of 12 ns FWHM and $\sim 5 \text{ mJ}$ of energy at 355 nm. The 355 nm pulses are sent through an optical delay line that introduces a delay of 5 ns between them and the jump pulses generated in the dye laser. The two beams are then spatially overlapped using a dichroic mirror and focused into the sample cell by the above mentioned $f = 450$ lens.

The reasons for using 355 nm as photodissociation wavelength require a more detailed explanation: Of all the states schematically displayed in Fig. 1, the $(0,0,4)$ state lies at $\sim 12\,630 \text{ cm}^{-1}$ above the ground state, the excited states we want to reach lie at $\sim 30\,000 \text{ cm}^{-1}$ and the $CN(A)$ state has an energy of $\sim 52\,800 \text{ cm}^{-1}$. This is, however, the energy at the outermost point of the ${}^1\Pi$ dissociative surface of HCN that leads to the production of $CN(A)$: for a bound-to-free transition arriving to this surface to have a non-negligible amplitude, the transition has to take place in the inner region of the surface, where the vibrational wave function of the bound state in which the transition originates has a significant value. This is the kind of transition displayed in Fig. 1: in a first approximation, it can be assumed that these transitions are going to take place only at distances shorter than

the outer turning point of the bound vibrational state. This increases the amount of energy necessary to reach the dissociative surface: since this surface is not well-known experimentally, based on the best available calculation⁸⁹ we estimated that for a transition departing from an excited vibrational state lying at $30\,000\text{ cm}^{-1}$ a minimum energy of $\sim 28\,200\text{ cm}^{-1}$ is required to reach dissociation, while a transition departing from the (0,0,4) state requires at least $\sim 45\,500\text{ cm}^{-1}$. These values set the approximate boundaries for the photodissociation wavelength between a minimum of 220 nm (shorter wavelengths would also produce dissociation from the (0,0,4) state) and a maximum of 354 nm (longer wavelengths would not have enough energy to photodissociate HCN from the highly excited states we want to reach). With these values in mind our first choice was to frequency-double a fraction of the jump laser beam (with wavelengths between 620 and 550 nm) and use it for photodissociation. This setup has the advantage of not requiring an additional light source to generate the photodissociation pulses. However, in our first experiment with this configuration we found that the use of photodissociation wavelengths around 300 nm had as a secondary effect the production of a significant amount of CN(A) photofragments even in the absence of the pump laser pulses. This could be easily verified by blocking the Ti:sapphire laser and checking that the probe beam was still able to induce a fluorescent emission from the CN(B) state, which is a clear proof of the presence of CN(A) radicals. The only possible mechanism for the production of CN(A) photofragments in the absence of the first vibrational excitation is a two-photon absorption from the ground state to the $^1\Pi$ dissociative electronic state of HCN. Although two-photon absorptions are several orders of magnitude weaker than direct absorptions, in this experimental configuration the amount of CN(A) photofragments produced through the two-photon absorption channel is not much smaller (approximately a factor of 4 or 5) than the amount produced by the sequential channel. The explanation resides in the fact that in the sequential channel each one of the vibrational excitation steps involves important losses: even although we work in a saturation or near saturation regime, only a small fraction of all the available population (not more than 5%) in the lower vibrational state of the transition is pumped to the more excited state, since only one rotational transition is being excited. The two-photon absorption, on the other hand, has the entire rotational population of the ground vibrational state available.

A quick check of the energy values estimated above reveals that any photodissociation wavelength shorter than 344 nm has enough energy to reach the $^1\Pi$ dissociative excited state of HCN from the ground vibrational state through a two-photon absorption.⁹⁰ With these values, the interval of usable wavelengths is roughly limited to the 344–354 nm range. This is the reason for our use of 355 nm radiation, since being close enough to the mentioned interval (its usability had to be experimentally verified) it is easy to obtain from a Nd:YAG laser.

The probe pulse is generated in a low-power dye laser (Molelectron DL-II) pumped by an N_2 laser (Molelectron UV-22). Typical values for its energy and duration are $300\ \mu\text{J}$

and 5 ns FWHM, with a spectral width of 0.4 cm^{-1} . A dichroic mirror is used to spatially overlap the beam with the first vibrational excitation beam, and the same lens ($f=360$) focuses them into the sample cell. The frequency of the laser was tuned to $18\,808\text{ cm}^{-1}$, which corresponds to the most intense region of the $\text{CN}(v=1,B)\leftarrow\text{CN}(v=0,A)$ vibrational band in thermal equilibrium,⁸¹ and was kept constant during all the experiments.

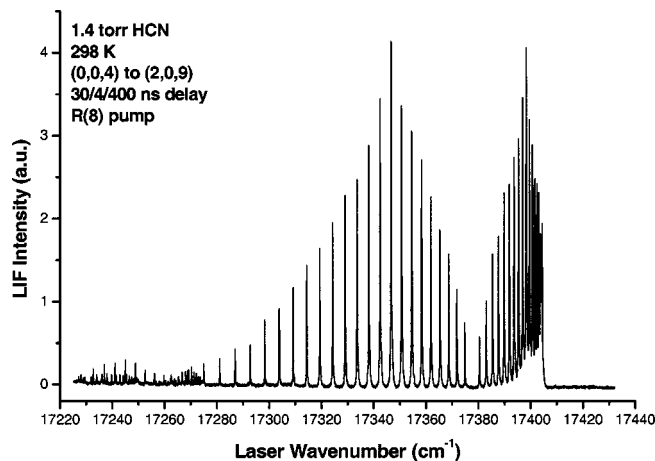
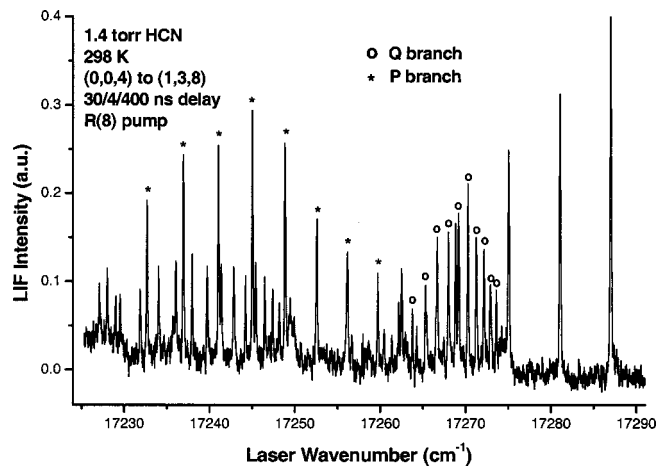
The sample cell, made of stainless steel, consists of a central, cubic section and two baffled side arms with UV-silica windows mounted at Brewster's angle. The total length of the cell is 34 cm. An UV-sensitive photomultiplier tube (EMI 9635QB) is mounted on one of the sides of the central section, perpendicular to the cell optical axis. The $\text{CN}(X)\leftarrow\text{CN}(B)$ fluorescent emission from the CN photofragments is collected by an $f=50$ mm lens and sent to the photomultiplier. A bandpass interference filter placed between the lens and the PMT, centered at 390 nm with a 10 nm FWHM, is used to block scattered light and insure that only fluorescence coming from the $X\leftarrow B$ transition is detected. A capacitance manometer (MKS 622 A02TAE) mounted on the central section of the cell monitors the sample pressure, between 1 and 3 Torr for most experiments. A single inlet-outlet orifice is used to fill the cell with HCN from a gas cylinder and evacuate it with a cryopump. HCN was synthesized prior to the experiment using a simple chemical procedure described elsewhere⁸⁰ and used without further purification. An FTIR spectrum of the synthesized sample was recorded to insure the absence of significant impurities.

The output of the photomultiplier is sent, without any intermediate amplification, to a gated integrator (SRS 250) and from there to a PC computer equipped with a data acquisition card (National Instruments AT-MIO-16X) that performs a 16 bit analog-to-digital conversion. Other signals of the experiment (laser power, photogalvanic spectrum, etalon transmission fringes) are also integrated and sent to the computer.

The delay between the different pulses participating in the experiment is controlled by an array of digital delay generators (SRS DG535) that act as master clock and externally trigger all the lasers. Except for the photodissociation pulse, which has a fixed optical delay of 5 ns with respect to the jump pulse, all the other delays can be adjusted at will, providing the experiment with a flexibility that can be used for a number of different studies.⁹¹

To get as much information as possible from the rovibrational spectra, it is necessary to make sure that there is enough number of collisions to populate a significant number of rotational states in (0,0,4). The required delay was empirically determined and, for most of our experiments, was set to a value between 30 and 45 ns. This, combined with sample pressures between 1 and 3 Torr, allowed us to observe a good number of rotational components in all the vibrational bands of the spectra. As for the delay between the photodissociation and probe pulses, it was set to 400 ns in all the experiments. This large delay is convenient for two reasons:

- The probe laser is tuned to excite the most intense region of the $\text{CN}(v=1,B)\leftarrow\text{CN}(v=0,A)$ vibrational band in thermal equilibrium, but since the rotational energy distribu-

FIG. 3. The (2,0,9) \leftarrow (0,0,4) band.FIG. 4. The (3,1,8) \leftarrow (0,0,4) band.

tion in the CN(A) photofragments immediately after their formation does not necessarily correspond to thermal equilibrium, part of the population that in equilibrium would contribute to the intensity of the region of the band excited by the laser resides now in higher rotational states. Previous measurements⁸¹ allowed us to determine that a delay between photodissociation and probe of 400–600 ns is enough for almost complete collisional rotational relaxation of the CN(A) radicals. In these conditions, the fluorescent emission induced by the probe laser is maximized.

- Despite the fact that a bandpass filter is used for the detection of the fluorescent emission, there is still a background signal due to light scattering induced by the photodissociation beam that reaches the photomultiplier. Since this background signal is associated with the photodissociation beam, short delays between photodissociation and probe result in $X\leftarrow B$ fluorescence signals that are “riding” on top of background scattering signals and thus strongly affected by the shot-to-shot noise of these signals, which reproduces the shot-to-shot noise of the photodissociation laser. Longer delays combined with gated integration remove most of this noise and dramatically improve the S/N ratio. The definition of “short” or “long” delay is determined in this case by the rise and decay times of the PMT, which produce a function with a FWHM of ~ 50 ns.

III. RESULTS

When the experimental setup described above was used to scan the region between 550 and 620 nm, a total of eight vibrational bands were found. Six of these bands show relatively simple PR or PQR rotational structures, allowing for a straightforward analysis that renders the rotational and vibrational parameters of the upper vibrational state of the transitions, while other exhibit complex rotational structures arising from the overlapping of different vibrational transitions and the presence of perturbations.

Figure 3 shows one of the most intense bands observed, identified as corresponding to the (2,0,9) \leftarrow (0,0,4) $\Sigma-\Sigma$ transition. The signal-to-noise ratio for the highest peaks of the spectrum in this figure is of the order of 150, but after a finer tuning of the experimental parameters values close to 500

were reached for this and the other $\Sigma-\Sigma$ band observed. Two main features are visible in the rotationally resolved spectrum: the first one is the particular shape of the R branch of the band, strongly congested for high J values. The branch does not converge to a limit, as its shape seems to suggest, but turns around at $J\approx 20$. This is due to the significant difference in the values of the B rotational constants of the lower and upper states of the transition, separated by seven vibrational quanta. The second most visible feature is the unusual relative intensities of the rotational components: both branches present a clear maximum for $J=9$, while the Boltzmann maximum for the (0,0,4) state is expected to occur for $J=8$. The reason for this discrepancy is found in the experimental conditions used for this particular measurement: The pump laser was tuned to the $R(8)$ component of the (0,0,4) \leftarrow (0,0,0) transition, thus populating only the $J=9$ level in the upper vibrational state, and the delay between the pump and jump lasers was set to 30 ns. This delay is long enough to allow a significant collisional relaxation that populates all the other rotational states that can be observed in our spectrum, but not long enough for the populations to reach thermal equilibrium, which explains why the most populated rotational state in our spectra is still the one that initially accumulated all the population, $J=9$.

The existence of a much weaker structure overlapped with the high- J components of the P branch can also be observed in Fig. 3. Figure 4 presents a more detailed view of this region, where it becomes evident that the structure has contributions from different vibrational bands. The dominant band is a PQR structure of which only the P and Q branches are clearly visible. The rotational lines of this band have been marked in Fig. 4 to facilitate their identification. The band was assigned to a $\Sigma-\Pi$ transition between the (0,0,4) and (3,1,8) states. Of special interest is the fact that the R branch is much weaker than it would be expected from the intensities of the P and Q branches, to the extent of being almost indistinguishable from the background noise in our spectra: Only a few very weak lines are visible in the region between 17 280 and 17 300 cm^{-1} where the R branch should be. The most likely explanation for this behavior is the presence of a perturber state near the (3,1,8). Moreover, and

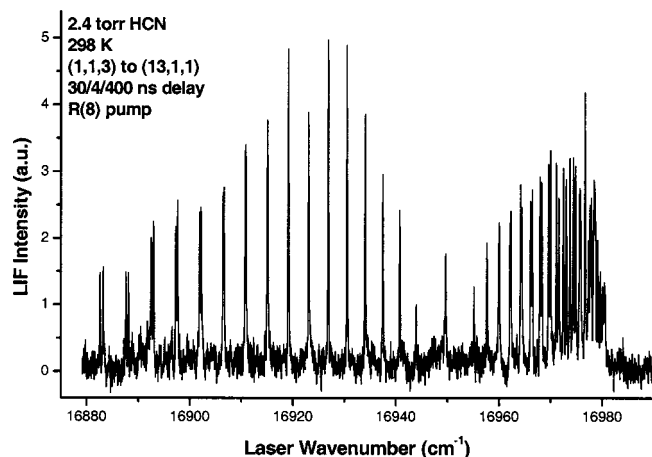


FIG. 5. The (13,1,1)←(1,1,3) band.

since the effect of the perturbation is different for the *P* and *R* branches, the symmetry of the perturber state has to be different from that of the (3,1,8) perturbed state.⁹²

Figure 5 presents a third type of vibrational band found in our spectra. In this case, a *PR* structure showing the above mentioned pattern of congestion in the *R* branch is accompanied by a very weak central *Q* branch, visible as a single line. The rotational lines of the *P* and *R* branches are doublets with a splitting between the components that increases with the rotational quantum number, which is consistent with an *l*-doubling pattern. A more detailed analysis of the rotational structure shows that the *P*(1) and *R*(0) lines are missing. These factors allow for an easy identification of the band type as corresponding to a Π – Π transition. The fact that this kind of transition is observed in our experiment is of particular interest: since the only vibrational state being populated by the pump laser is the (0,0,4), with Σ symmetry, the departure vibrational state for these Π – Π transitions has to be populated by some other mechanism, that can only be collisional relaxation from the (0,0,4) to a nearby Π state. This state was identified as (1,1,3), lying ~ 309 cm^{-1} below the (0,0,4).

Finally, Fig. 6 presents an example of one of the more

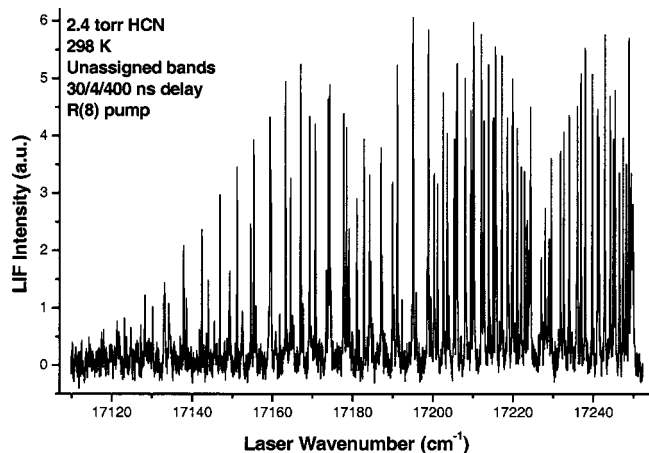


FIG. 6. Unassigned band.

complex structures that have also been recorded. The analysis of these bands is still in progress and has not been included in this work.

For the identification of the observed bands we supplement our analysis with results from a variational calculation using the Carter–Handy–Mills potential.⁹³ This potential was refined from data for HCN and DCN which were available before 1990, plus the more recent data of Yang, Rogaski, and Wodtke covering high bending levels of HCN.³⁶ We have already used this potential to confirm the assignments of weak overtone bands in the range 19 528–23 048 cm^{-1} ,⁴³ for which the theoretical and experimental assignments fully agree, and for which the mean theoretical vibrational error is only 2.5 cm^{-1} . We consider it appropriate, therefore, to attempt calculations to 30 000 cm^{-1} using this potential in order to locate and assign the new observed bands.

The variational calculations are based on a kinetic-energy operator in internal valence coordinates⁹⁴ and uses a potential energy function in these coordinates, expressed in terms of Morse-type polynomial terms for the HC and CN stretches and angular displacements terms for the bend, with the recently refined equilibrium geometry as Ref. 95. The primitive basis is similarly defined by Morse functions and associated Legendre functions, respectively, in the same valence coordinates. There are two important features of this calculation that make reliable assignments possible for quite high energies. First, the primitive basis is not established in pure HC or CN stretch coordinates, but in those associated with the eigenfunctions of a two-dimensional FG diagonalization.⁹⁶ This ensures that the coordinates behave very much like the stretch normal modes for near-equilibrium configurations. Second, initial contractions of the stretch and bend primitives take place using effective Hamiltonians with the nonparticipating coordinates frozen at their equilibrium values. The resulting eigenfunctions (two-dimensional in stretch and one-dimensional in bend) then label the stretch and bend quanta in a subsequent three-dimensional vibrational calculation (for which the Hamiltonian matrix becomes progressively more diagonal) providing the contracted levels can themselves be accurately assigned.

The labeling of the contracted bend quanta is trivial, and is merely the ordering of a one-dimensional stack of functions of increasing energy. That of the contracted stretch quanta is not that easy, especially for high-energy eigenfunctions, where heavy mixing of the primitive basis occurs. For low-lying levels, our choice of stretch coordinates ensures that the stretch–contraction Hamiltonian matrix is almost diagonal, and this persists to rather high energies. However, for high stretch energies, we make use of an independent assignment obtained by continuation of known lower energy vibrational series used to assign calculated levels involving only stretching excitation. There are no assignments from this procedure that differ from those that are unambiguous from inspection of the stretch eigenvectors, which lends support to the validity of those for the remaining levels. This means that the assignments associated with the majority of all functions entering the vibrational Hamiltonian are known, and pro-

TABLE I. Bands and band origins.

Band structure	Transition	Origin (cm ⁻¹)	Calculated (cm ⁻¹)	Fitted lines
<i>PQR</i> (Σ - Π)	(13,1,1) \leftarrow (0,0,4)	16 640.72(5)	16 635.82	22
<i>PR</i> (Σ - Σ)	(3,0,8) \leftarrow (0,0,4)	16 731.31(3)	16 718.73	43
<i>PQR</i> (Π - Π)	(13,1,1) \leftarrow (1,1,3)	16 949.75(4)	16 944.49	50
<i>PQR</i> (Σ - Π)	(3,1,8) \leftarrow (0,0,4)	17 276.6(1)	17 271.12	18
<i>PR</i> (Σ - Σ)	(2,0,9) \leftarrow (0,0,4)	17 377.72(3)	17 363.43	40
<i>PQR</i> (Π - Π)	(3,1,8) \leftarrow (1,1,3)	17 585.4(1)	17 579.79	35

vided that large resonances are absent, the vibrational levels are also clearly assigned. Our assignments are based on the single largest coefficient in the three-dimensional eigenvectors for all the Σ levels of interest (these were all >0.9 and unambiguous).

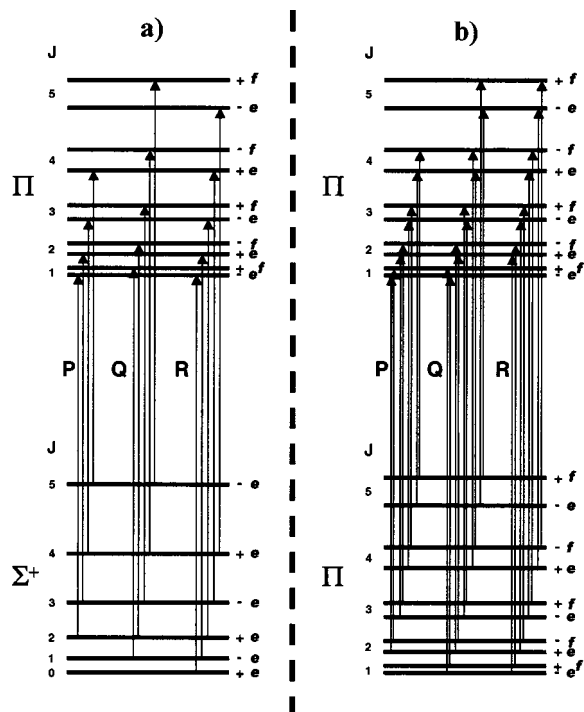
For the Π levels, two three-dimensional calculations take place with $K_a = 0, 1$ where the expansion set is augmented by symmetric top Wang combinations for the rotational functions. Eigenfunctions of these diagonalisations are finally mixed through terms off-diagonal in K_a .⁹⁴ If the Σ levels are all correctly assigned, the Π levels usually present no problem, where coefficients of >0.9 in the rovibrational eigenvectors are again found.

Our calculations used 38 stretch primitives and 49 bend primitives, which were integrated numerically by Gauss quadrature with 56 and 66 points, respectively. From the resulting stretch contraction, 204 of the possible 1444 two-dimensional functions were selected, for which we could assign the lowest 152. For the one-dimensional bend contraction, 14 functions (26 bending quanta) were carried forward. The vibrational matrices were, therefore, of order 2856 from which 2000 were used in the rovibrational matrices (orders 4000 for “e”, 2000 for “f”). These were sufficient to converge all required levels to better than 0.001 cm^{-1} and all assignments were unambiguous.

Table I summarizes the types, assignments and origins of the six bands analyzed for this work, together with their calculated origins and the number of lines fitted for each band. The predictions provided by the calculation, combined with the information contained in the symmetry and intensity of the observed bands, made the task of identifying the upper vibrational states of these bands a relatively simple one in most cases, but given the high density of states in this high-energy region a certain degree of caution is in order. To verify the feasibility of our assignments we carried out an analysis of the vibrational dependence of the rotational constants of these states: using the values calculated in Ref. 34 for the different α and γ constants that are normally used to express this vibrational dependence, we calculated values for the B_v rotational constants of the five states we believe to be responsible for the bands we observe, and compared these values with the ones obtained from the fitting of the bands. The agreement was satisfactory for four of the five observed states: The two Σ states (with differences obs-calc of the order of $5 \times 10^{-3} \text{ cm}^{-1}$), the (1,1,3) Π state (o-c $\sim 4 \times 10^{-4} \text{ cm}^{-1}$) and the (3,1,8) Π state (o-c $\sim 1 \times 10^{-2} \text{ cm}^{-1}$). While some of these differences—especially the one for the (3,1,8) state—may seem large, it must be noted that the calculated constants have been computed by means of an extrapolation

that uses values of α and γ constants obtained from states with relatively low vibrational excitation: Most of the states used in Ref. 34 for the fitting of the α s and γ s had between 1 and 3 quanta of vibrational excitation, and only a few of them had more than that (typically localized in the ν_3 mode). This limits the accuracy one can expect from this extrapolation at high energies. Despite this limitation, the extrapolated values are still useful, when combined with the information of the symmetry of the bands, to provide some idea of the feasibility of the assignments and limit the number of other possible candidate states: for example, if our assignments of any of the Σ states were incorrect, other candidates would be states with an even number of bending quanta (0,2,4,...) in this energy region. But given the strong dependence of the rotational constant of the state with the number of bending quanta, the extrapolation shows that states with a high number of bending quanta would have values of B much larger than the experimental one, and can be eliminated. Thus from the extrapolated values of the B constants it can be inferred that only states with a low number of bending quanta (0 or 2) are reasonable candidates for the assignment. The same argument can be made for the Π states with the only difference of an odd number (1 or 3) of bending quanta. This is of great help when making or confirming the assignments, since although the density of states is high in this energy region, the density of states with a given symmetry and a low number of bending quanta, that would have values of their B rotational constants close to the observed—and calculated—ones, is much smaller. Thus the results of the extrapolation confirm, if not the certainty, at least the feasibility of our assignments for the states mentioned above.

For the Π state we have labeled (13,1,1) the obs-calc difference is of $4 \times 10^{-2} \text{ cm}^{-1}$, much larger than for any of the other states. This is a disturbing result that seems to indicate that our assignment for this state is wrong, but although the calculation predicts other states of Π symmetry in the region nearby none of them seems to be a more suitable candidate than (13,1,1). It is certainly possible that the reason for part of this large obs-calc error is the lack of accuracy of the extrapolation for states with high excitation in the ν_1 mode: as mentioned before, most of the states used in Ref. 34 for the fitting of the α s and γ s had a low number of quanta of vibrational excitation, and none of them had more than 3 in the ν_1 mode (compared to a maximum of 6 in the ν_3 mode). From this, it is to be expected that predictions of rotational constants for states with a high number of quanta in the ν_1 mode will be much poorer than predictions for states where the energy is mostly localized in the ν_3

FIG. 7. Splitting patterns for Σ - Π and Π - Π bands in HCN.

mode. Even if this is the case, however, the experimental value of the rotational constant of this state seems suspiciously large for a state with 14 quanta of stretch excitation. It is thus advisable to exercise caution and, while we have maintained the (13,1,1) label in our tables as the most likely identity of the observed state, one should be aware that this particular assignment is not solid.

The analysis of the rotational information contained in the spectra was done individually for each one of the bands. The fitting of the Σ - Σ bands is completely straightforward, while the Σ - Π and Π - Π bands are slightly more complicated due to the fact that the double degeneracy of the Π states is broken by Coriolis interactions, giving rise to "parity doublets." This situation is represented, for the HCN molecule, in Figs. 7(a) (Σ - Π) and 7(b) (Π - Π), where the "e" and "f" notation⁹⁷ has been used to label the states. It must be noted that for relatively well studied molecules like HCN, for which the symmetry of the different wave functions (electronic, vibrational, rotational...) is known, the parity of the states is also well known, and the assignment of the "e" and "f" labels is trivial. The parity selection rule ($+\leftrightarrow-$ for dipole transitions) can be translated in terms of "e" and "f" as $e\leftrightarrow f$ for Q branches and $e\leftrightarrow e$ $f\leftrightarrow f$ for P and R branches.

It can be seen that for a Σ - Π band, as a consequence of the splitting in the upper states, transitions belonging to the Q branch always arrive to the upper components of the parity doublets while transitions belonging to the P and R branches arrive to the lower components of the doublets. This has to be taken into account in the analysis or different B' constants will be obtained from different branches. For a Π - Π band, the consequence of this splitting in both the upper and the lower states is the existence of two transitions of slightly different frequency (l -doubling), that—if analyzed indepen-

dently—would yield two slightly different sets of rotational constants

A least-squares fit was done for each assigned band using the following well-known expressions for the transition wave numbers:

1. Σ - Σ bands:

$$\nu = \nu_0 + m^4(D'' - D') - 2m^3(D'' + D') + m^2(B' - B'' + D'' - D') + m(B' + B''), \quad (1)$$

with $m = -J$ for the P branch and $m = J + 1$ for the R branch.

2. Σ - Π bands:

(a) For the P and R branches

$$\nu = \nu_0 - B'l^2 + m^4(D'' - D') - 2m^3(D'' + D') + m^2\left(B' - B'' + D'' - D' + \frac{q'}{2}\right) + m\left(B' + B'' + \frac{q'}{2}\right), \quad (2)$$

where m has the same meaning as in the previous expression, l is the vibrational angular momentum (1 in all our cases) and q' is the splitting parameter for the Π state (often called l -doubling parameter, although the name is not appropriate for a Σ - Π transition). The assumption made for our analysis is that the splitting of the rotational levels of the Π state is symmetric and described by the usual expression

$$\Delta\nu = q'J(J+1). \quad (3)$$

(b) For the Q branch

$$\nu = \nu_0 - B'l^2 + J^4(D'' - D') + 2J^3(D'' - D') + J^2\left(B' - B'' + D'' - D' - \frac{q'}{2}\right) + J\left(B' - B'' - \frac{q'}{2}\right). \quad (4)$$

3. Π - Π bands:

(a) For the P and R branches

$$\nu = \nu_0 - B'l^2 + B''l^2 + m^4(D'' - D') - 2m^3(D'' + D') + m^2\left(B' - B'' + D'' - D' \pm \frac{q'}{2} \mp \frac{q''}{2}\right) + m\left(B' + B'' \pm \frac{q'}{2} \pm \frac{q''}{2}\right), \quad (5)$$

where the parameters have the same meaning as above and a new one, q'' , has been introduced to account for the splitting in the lower Π state. The \pm and \mp signs in the last equation imply that two different fits have to be carried out independently, one for each set of l -doublet components. Given the low intensity of the Q branches of these transitions, no attempt was made to extract any information from them.

(b) For the parity splitting

$$\Delta\nu = m^2(q' - q'') + m(q' + q''), \quad (6)$$

where $\Delta\nu$ represents the frequency difference between the two components of a given doublet. The only use of this equation is to allow an independent determination of the l -doubling parameters that is not influenced by the other rotational constants involved in a higher-order fitting.

TABLE II. Energies and rotational constants.

State	G_v^{calc} (cm ⁻¹)	G_v (cm ⁻¹)	B_v (cm ⁻¹)	D_v (cm ⁻¹)	q_v (cm ⁻¹)
(1,1,3)	12 328.66	12 328.3(1)	1.4411(6)	$(2.9 \pm 1.2) \times 10^{-6}$	-0.0079(4)
(13,1,1)	29 273.08	29 277.98(5)	1.3746(4)	$(2.9 \pm 1.4) \times 10^{-6}$	-0.0108(4)
(3,0,8)	29 354.62	29 367.20(3)	1.366 67(5)	$(2.40 \pm 0.09) \times 10^{-6}$...
(3,1,8)	29 908.38	29 913.8(1)	1.378(1)	...	-0.0054(5)
(2,0,9)	29 999.32	30 013.61(3)	1.361 29(5)	$(2.25 \pm 0.09) \times 10^{-6}$...

Some of the criteria used in these equations require further clarification. For the Σ - Π bands:

- Our band origins ν_0 are calculated according to the definition in Eqs. (2) and (4), that is, they do not include the $-B'l^2$ factor. This has to be taken into account if our results are to be compared to theoretical predictions or other authors' results, since it is not unusual to include the mentioned factor into the band origin.

- The q' splitting parameter was introduced into the equations with a sign such that a positive value of q' would mean that transitions belonging to the P and R branches would arrive to the upper components of the doublets while Q -branch transitions would arrive to the lower ones. Since this is the opposite case of the one described in Fig. 7(a), which is known to be the "normal" case for HCN, in the absence of perturbations that could modify this pattern a negative value of q' is expected.

Finally, the Π - Π bands follow the criteria:

- The band origins are calculated according to (5), not including the $(B''-B')l^2$ term.

- The q' and q'' splitting parameters have been introduced in the equations (for the P and R branches only) with signs that assume a "symmetric" behavior for the transitions, that is, a transition departing from the upper component of a doublet in the lower Π state arrives to the upper component of the doublet in the upper Π state, and a transition departing from the lower component of a doublet arrives to the lower component of the doublet in the destination Π state. Since this is the expected pattern for HCN, as represented in Fig. 7(b), the relative signs of q' and q'' obtained from the fitting should be the same, either both positive or negative. Whether the absolute sign is positive or negative cannot be determined from the Π - Π transitions.

The positions of the states participating in the analyzed transitions are summarized in Table II together with their calculated values and the rotational constants obtained from the fits. The energy values given in this table correspond to the energy of the lowest rotational state of that vibrational state, that is, $J=0$ for states of Σ symmetry and $J=1$ for states of Π symmetry.

IV. DISCUSSION

The most noticeable feature of the data displayed in Table II is the high vibrational excitation of the states observed, up to 15 quanta of vibrational excitation mainly localized in the stretching coordinates, with energies between 29 000 and 30 000 cm⁻¹. This is more than 2/3 the dissociation energy D_0 of HCN in its ground electronic state,⁹⁸

$\sim 43\,740$ cm⁻¹. The observation of these states constitutes an important extension of the existing experimental data.

The centrifugal distortion constants D_v could only be determined accurately for the two states participating in Σ - Σ transitions. Since these were the most intense bands, a large number of rotational lines could be observed, which together with the fact that the lower state of these transitions is well known allowed the fitting of these constants. For the (13,1,1) \leftarrow (1,1,3) Π - Π band a large number of components was also observed (30 different rotational transitions for 20 of which the l -doublets could be resolved), thus allowing the determination—although not as precise as for the Σ states—of the distortion constants. For the weaker Σ - Π transitions, the number of observed rotational components was not enough for a statistically significant estimate of these constants.

The splitting parameters q_v were determined for the three vibrational states with Π symmetry observed. The "−" signs of these parameters are a consequence of the way they were introduced in the equations: the symmetry of the splittings follows the patterns displayed in Fig. 7 in all the cases.

The (3,1,8) \leftarrow (1,1,3) Π - Π band presents a particularly interesting feature: Due to the presence of a nearby state, a perturbation occurs that alters the l -doubling pattern in both branches, shifting the positions of the "e" components of the doublets while the "f" components remain unaltered. This clearly identifies the perturbation as a Coriolis interaction with a perturber state of Σ symmetry. A crossing occurs between $J=11$ and $J=12$. Since the "f" components remain unchanged by this perturbation, rotational constants for the unperturbed band could still be obtained. An analysis of the perturbation was also carried out and the constants of the perturber Σ state as well as the interaction term W^2 were calculated. These constants are presented in Table III. Since no transitions to the perturber state were clearly observed the determination is not very precise.

A second perturbation was also visible near the center of the band, affecting only the low- J components ($J=1$ to $J=4$) of both branches. The nature of this perturbation is different from the previous one: it affects both symmetry components of the doublets, which leaves two main possibilities: First, it could be due to the presence of a Coriolis

TABLE III. Constants of the perturber states.

Symmetry	G_v (cm ⁻¹)	B_v (cm ⁻¹)	W^2 (cm ⁻²)
Σ	29 922(2)	1.31(1)	0.0021(3)
Π	29 913(1)

resonance with a nearby Δ state. This, however, is not consistent with the fact that the $J=1$ components are also perturbed. The perturbation is thus likely to be due to the second possibility, an anharmonic resonance with a neighboring Π state. Since some lines due to transitions involving the perturber were visible in the spectrum, its energy G_v could be determined with a slightly better precision than that of the perturber Σ state and is also given in Table III.

A tentative identification of these perturber states has been carried out with the assistance of the variational calculation mentioned earlier. For the identification of the Σ perturber the calculation provides two suitable candidates in the vicinity of the experimentally observed state. The first one is (12,0,2), with a calculated energy of 29 898 cm^{-1} , although the difference between this value and the experimental one (24 cm^{-1}) seems too large when compared with the typical differences between observed and calculated energies in Table II, which are, for the worst cases, of 14 cm^{-1} for the Σ states in this region of the spectrum. The second candidate has a calculated energy much closer to the experimental value, 29 925 cm^{-1} , and corresponds to a heavily mixed state with the largest contribution (a coefficient of 0.38) coming from the (9,4,3) Σ state. All the other states contributing to this mixture have a very high number of CN quanta. The small value of the rotational constant determined from the spectrum seems to point to a state with a large number of CN quanta, a condition which both candidates fulfill. Based on the calculated energies for these states the highly mixed state we have labeled (9,4,3) seems more likely to be the perturber, but no definitive answer can be given with the information available.

Identification of the Π perturber state is even more problematic. The most likely candidate with that symmetry emerging from the calculation is a heavily mixed state with an energy of 29 904 cm^{-1} , but due to the mixing its assignment is uncertain: The largest contribution to this state comes from (8,7,3), with a coefficient of 0.28, but there are also significant contributions from (10,13,0), (9,11,1), (12,11,0), (11,9,1), and (7,7,4), with coefficients of 0.22, 0.22, 0.21, 0.20, and 0.19. It is thus nearly impossible to venture any assignment with a reasonable level of certainty.

It may surprise that S/N ratios as high as 500 could be obtained for some of the spectra when the states involved in the transitions are separated by seven or more vibrational quanta and the departure state is already an excited state. To achieve these ratios, a careful optimization had to be carried out for each one of the four experimental steps. The first two steps, involving population transfer between rovibrational states, required the use of very high powers that allowed us to work in a near-saturation regime. While for the first step (0,0,4) \leftarrow (0,0,0) this was always true, for the second vibrational excitation only the most intense transitions of the two Σ - Σ bands were close to this regime. The photodissociation beam was also optimized in power and wavelength, as described in the experimental section, to minimize background signals. Finally, a very sensitive detection scheme (LIF) was used also in a near-saturation regime. Even with these optimizations, it must be noted that the S/N ratios of this experiment would have been worse if a molecule with smaller an-

harmonicity had been studied: the high anharmonicity of HCN greatly increases the efficiency of the “jump” stage and is a key factor to the success of the experiment.

The observation of Π - Π bands in the spectra was unexpected, but once the bands were assigned and the departure state identified the interpretation was straightforward: due to collisional relaxation, population “falls” from the excited (0,0,4) state to the (1,1,3) state, roughly 309 cm^{-1} below, and transitions departing from this state can be observed. This interpretation was confirmed by the changes observed in the spectra when the experimental conditions were modified: for the Σ - Σ and Σ - Π bands, it was empirically determined that the maximum amount of fluorescence signal was obtained at a sample pressure of ~ 1.4 Torr. Lower pressures decreased the efficiency of the vibrational population transfer, while at higher pressures fluorescence quenching became noticeable. For the Π - Π bands, on the other hand, this maximum was found to be at a sample pressure of ~ 2.4 Torr, which clearly indicates that there is some other process involved in the observation of these bands, a process whose efficiency is being increased by this higher sample pressure to the extent of compensating for the signal loss due to fluorescence quenching. This process is collisional relaxation.

The high efficiency of collisional relaxation in HCN has been thoroughly studied by other authors;^{52,53} it is a direct consequence of its large dipole moment, which allows HCN molecules to “feel” the presence of each other and interact at large distances. If we assume that the absorption cross sections for the transitions in the Π - Π bands we have observed are similar to the cross sections of those in the Σ - Σ bands (which is a reasonable assumption considering that the change of vibrational quanta in these transitions is also similar), then an approximate idea of the amount of population transferred by collisions can be extracted just from the different S/N ratio in both types of bands. In our case, the Σ - Σ bands are roughly 30–50 times more intense than the Π - Π bands, which yields an estimation of 2%–3% of the population in (0,0,4) transferred to (1,1,3). If we consider that this transfer takes place during a time of only 30 ns at a sample pressure of 2.4 Torr and to a state located 309 cm^{-1} away, it becomes qualitatively very clear that vibrational collisional relaxation is an extremely efficient mechanism in HCN.

The comparison between the calculated and the experimentally determined positions of the vibrational states is not quite of the same quality as that obtained for our earlier experiments,^{43,93} with a mean error of 7.5 cm^{-1} (cf. 2.5 cm^{-1}). However, for both of these comparisons, the calculations did not include any of the relevant data in the fit, and must be viewed as predictions from our earlier refinement. This said, our aim was mainly to confirm the experimental assignments, which we have been able to do. We also believe that the agreement for such highly excited vibrational levels is sufficiently good for us to be in a position to refine the HCN potential at some later stage, using our earlier potential⁹³ as starting point, and with the results of this and our earlier work⁴³ included in the least-squares fit.

V. CONCLUSIONS

An experimental setup has been built that, based on the use of vibrationally mediated photodissociation, allows the study of highly excited vibrational states of molecules in gas phase up to energies as high as $30\,000\text{ cm}^{-1}$. This scheme is particularly attractive when applied to the study of highly anharmonic vibrations, since these tend to show stronger overtone transitions.

The experimental setup has been applied to the study of vibrationally excited states in the ground electronic state of the molecule of HCN. As a result, eight vibrational bands have been observed for the first time, of which six have been analyzed, rendering molecular parameters for four highly excited vibrational states located in the region between $29\,000$ and $30\,000\text{ cm}^{-1}$. This is, to our knowledge, the first experimental observation of these states. Analysis of the two remaining bands is in progress.

The identification of the vibrational states was assisted by comparison with the results of a state-of-the-art variational calculation based on the Carter–Handy–Mills potential. The agreement between theory and experiment is quite satisfactory, especially considering that we are dealing with highly excited states and a considerable extrapolation from the energy of the states used to fit the potential.

We would like to close with some observations on how the present work could be extended. Given the excellent signal to noise ratios observed in the present work, significantly higher vibrational states should be detectable by the same excitation scheme. The LIF detection step is limited by photon counting noise, and the total LIF could be significantly improved if a broad bandwidth dye laser were used for the excitation of CN(*A*) products, so that a sizable fraction of the total population could be probed instead of just a few rotational levels that lie near the band head of the *A*→*B* transition. Addition of a tunable near-IR laser would allow further excitation from levels in the $30\,000\text{ cm}^{-1}$ region to levels up to just below the dissociation threshold or even resonance states slightly above it. Crim and co-workers have studied the hydrogen extraction from the HCN (0,0,4) state with O, H, and Cl atoms.⁹⁹ These correspond to “chain propagation” reactions. The present work, that populates states with 2.5 times the vibrational energy of that earlier work, should allow the study of hydrogen extraction by molecules such as O₂ and NO, which would correspond to “chain initiation” reactions.

If the experiment were performed in a pulsed jet apparatus, one would remove most of the collisional relaxation observed in the present experiment. This would reduce the range of rotational states that could be studied for the highly excited states, but would improve the ability to use the power of double resonance to assign rotational structure for highly perturbed bands. Without extensive collisional reactions, one could use Stark quantum beat spectroscopy to measure the dipole moment of these highly excited vibrational states via modulations in the photodissociation yield as a function of an electric field times the time interval between jump and dissociation laser pulses.¹⁰⁰ It has been proposed that measurements of dipole moments would provide a sensitive

probe for states delocalized between HCN and HNC wells.¹⁰¹

ACKNOWLEDGMENTS

We are indebted to Dr. Paul Rabinowitz for his assistance in the assembly of the experimental setup: without his experience, the numerous and helpful discussions, and the many pieces of equipment we borrowed from him, this experiment would not have been possible. This work was supported by grants from the U.S. National Science Foundation and from the Petroleum Research Fund administered by the American Chemical Society. S.C. acknowledges support from the U.S. Office of Naval Research. R.Z.M. acknowledges the financial support provided by the Spanish Ministry of Education through a postdoctoral fellowship.

- ¹T. Ridgway, D. F. Carbon, and D. N. B. Hall, *Astrophys. J.* **225**, 138 (1978).
- ²W. Burmeister, *Verh. Dtsch. Phys. Ges.* **15**, 589 (1913).
- ³E. F. Barker, *Phys. Rev.* **23**, 200 (1924).
- ⁴R. M. Badger and J. L. Binder, *Phys. Rev.* **37**, 800 (1931).
- ⁵K. N. Choi and E. F. Barker, *Phys. Rev.* **42**, 777 (1932).
- ⁶A. Adel and E. F. Barker, *Phys. Rev.* **45**, 277 (1934).
- ⁷F. Bartunek and E. F. Barker, *Phys. Rev.* **48**, 516 (1935).
- ⁸E. Lindholm, *Z. Phys.* **108**, 454 (1938).
- ⁹In this work, we will use Herzberg's notation for labeling the vibrational modes: (ν_1, ν_2, ν_3) = (CN stretch, bending mode, CH stretch). Many authors invert the labels of the two stretching modes to be consistent with modern conventions.
- ¹⁰G. Herzberg, in *Molecular Spectra and Molecular Structure Vol. II. Infrared and Raman Spectra of Polyatomic Molecules* (Van Nostrand, Princeton, 1945).
- ¹¹W. C. Price, *Phys. Rev.* **46**, 529 (1934).
- ¹²H. J. Hilgendorff, *Z. Phys.* **95**, 781 (1935).
- ¹³W. C. Price and A. D. Walsh, *Trans. Faraday Soc.* **41**, 381 (1945).
- ¹⁴G. Herzberg and K. K. Innes, *Can. J. Phys.* **35**, 842 (1957).
- ¹⁵A. E. Douglas and D. Sharma, *J. Chem. Phys.* **21**, 448 (1953).
- ¹⁶G. E. Hyde and D. F. Hornig, *J. Chem. Phys.* **20**, 647 (1952).
- ¹⁷R. E. Kagaris, H. D. Rix, and D. H. Rank, *J. Chem. Phys.* **20**, 1437 (1952).
- ¹⁸A. G. Maki and L. R. Blaine, *J. Mol. Spectrosc.* **12**, 45 (1964).
- ¹⁹A. G. Maki, *Appl. Phys. Lett.* **12**, 122 (1968).
- ²⁰A. G. Maki, W. B. Olson, and R. L. Sams, *J. Mol. Spectrosc.* **36**, 433 (1970).
- ²¹G. Winnewisser, A. G. Maki, and D. R. Johnson, *J. Mol. Spectrosc.* **39**, 149 (1971).
- ²²A. G. Maki, *J. Mol. Spectrosc.* **58**, 308 (1975).
- ²³A. G. Maki, *J. Appl. Phys.* **49**, 7 (1978).
- ²⁴R. E. Bruns and W. B. Person, *J. Chem. Phys.* **53**, 1413 (1970).
- ²⁵R. E. Bruns and B. de Barros Neto, *J. Chem. Phys.* **68**, 847 (1978).
- ²⁶K. Kim and W. T. King, *J. Chem. Phys.* **71**, 1967 (1979).
- ²⁷P. R. Bunker and J. M. R. Stone, *J. Mol. Spectrosc.* **41**, 310 (1972).
- ²⁸G. Strey and I. M. Mills, *Mol. Phys.* **26**, 129 (1973).
- ²⁹J. N. Murrell, S. Carter, and L. O. Halonen, *J. Mol. Spectrosc.* **93**, 307 (1982).
- ³⁰K. K. Lehmann, G. J. Scherer, and W. Klemperer, *J. Chem. Phys.* **77**, 2853 (1982).
- ³¹A. M. Smith, K. K. Lehmann, and W. Klemperer, *J. Chem. Phys.* **85**, 4958 (1982).
- ³²A. M. Smith, U. G. Jørgensen, and K. K. Lehmann, *J. Chem. Phys.* **87**, 5649 (1987).
- ³³H. Sasada, *J. Chem. Phys.* **88**, 767 (1988).
- ³⁴A. M. Smith, S. L. Coy, W. Klemperer, and K. K. Lehmann, *J. Mol. Spectrosc.* **134**, 134 (1989).
- ³⁵A. M. Smith, W. Klemperer, and K. K. Lehmann, *J. Chem. Phys.* **90**, 4633 (1989).
- ³⁶X. Yang, C. A. Rogaski, and A. M. Wodtke, *J. Chem. Phys.* **92**, 2111 (1990).
- ³⁷X. Yang and A. M. Wodtke, *J. Chem. Phys.* **93**, 3723 (1990).

- ³⁸Z. Bazic and J. C. Light, *J. Chem. Phys.* **86**, 3065 (1987).
- ³⁹P. Botschwina, *J. Chem. Soc., Faraday Trans. 2* **84**, 1263 (1988).
- ⁴⁰J. E. Baggot, G. L. Caldow, and I. M. Mills, *J. Chem. Soc., Faraday Trans. 2* **84**, 1407 (1988).
- ⁴¹J. P. Brunet, R. A. Friesner, R. E. Wyatt, and C. Leforestier, *Chem. Phys. Lett.* **153**, 425 (1988).
- ⁴²P. R. Fleming and J. S. Hutchinson, *J. Chem. Phys.* **90**, 1735 (1989).
- ⁴³D. Romanini and K. K. Lehmann, *J. Chem. Phys.* **99**, 6287 (1993).
- ⁴⁴J. Preusser and A. G. Maki, *J. Mol. Spectrosc.* **162**, 484 (1993).
- ⁴⁵W. Quapp, S. Klee, G. C. Mellau, S. Albert, and A. Maki, *J. Mol. Spectrosc.* **167**, 375 (1994).
- ⁴⁶A. Maki, W. Quapp, and S. Klee, *J. Mol. Spectrosc.* **171**, 420 (1995).
- ⁴⁷A. Maki, W. Quapp, S. Klee, G. C. Mellau, and S. Albert, *J. Mol. Spectrosc.* **174**, 365 (1995).
- ⁴⁸A. Maki, W. Quapp, S. Klee, G. C. Mellau, and S. Albert, *J. Mol. Spectrosc.* **180**, 323 (1996).
- ⁴⁹A. Maki, W. Quapp, S. Klee, G. C. Mellau, and S. Albert, *J. Mol. Spectrosc.* **185**, 356 (1997).
- ⁵⁰A. G. Maki, G. C. Mellau, S. Klee, M. Winnewisser, and W. Quapp, *J. Mol. Spectrosc.* **202**, 67 (2000).
- ⁵¹M. Lecoutre, F. Rohart, T. R. Huet, and A. G. Maki, *J. Mol. Spectrosc.* **203**, 158 (2000).
- ⁵²J. S. Baskin, A. Saury, and E. Carrasquillo, *Chem. Phys. Lett.* **214**, 257 (1993).
- ⁵³R. Huang, J. Wu, M.-X. Gong, A. Saury, and E. Carrasquillo, *Chem. Phys. Lett.* **216**, 108 (1993).
- ⁵⁴D. E. Milligan and M. E. Jacox, *J. Chem. Phys.* **39**, 712 (1963).
- ⁵⁵D. E. Milligan and M. E. Jacox, *J. Chem. Phys.* **47**, 278 (1967).
- ⁵⁶L. E. Snyder and D. Buhl, *Bull. Am. Astron. Soc.* **3**, 388 (1971).
- ⁵⁷L. E. Snyder and D. Buhl, *Ann. N.Y. Acad. Sci.* **194**, 17 (1972).
- ⁵⁸A. G. Maki and R. L. Sams, *J. Chem. Phys.* **75**, 4178 (1981).
- ⁵⁹C. A. Arrington and E. A. Ogrzylo, *J. Chem. Phys.* **63**, 3670 (1975).
- ⁶⁰R. J. Saykally, P. G. Szanto, T. G. Anderson, and R. C. Woods, *Astrophys. J. Lett.* **204**, L143 (1976).
- ⁶¹G. L. Blackmann, R. D. Brown, P. D. Godfrey, and H. I. Gunn, *Nature (London)* **261**, 395 (1976).
- ⁶²R. A. Creswell, E. F. Pearson, M. Winnewiser, and G. Winnewiser, *Z. Naturforsch. A* **31**, 221 (1976).
- ⁶³E. F. Pearson, R. A. Creswell, M. Winnewiser, and G. Winnewiser, *Z. Naturforsch. A* **31**, 1394 (1976).
- ⁶⁴M. J. Winter and W. J. Jones, *J. Mol. Struct.* **80**, 43 (1982).
- ⁶⁵J. B. Burkholder, A. Sinha, P. D. Hammer, and C. Howard, *J. Mol. Spectrosc.* **126**, 72 (1987).
- ⁶⁶T. Okabayashi and M. Tanimoto, *J. Chem. Phys.* **99**, 3268 (1993).
- ⁶⁷F. J. Northrup, G. A. Bethardy, and R. Glen Macdonald, *J. Mol. Spectrosc.* **186**, 349 (1997).
- ⁶⁸T. A. Holme and J. S. Hutchinson, *J. Chem. Phys.* **83**, 2860 (1985).
- ⁶⁹Z. Bacic, R. B. Gerber, and M. A. Ratner, *J. Phys. Chem.* **90**, 3606 (1986).
- ⁷⁰R. S. Smith, R. B. Shirts, and C. W. Patterson, *J. Chem. Phys.* **86**, 4452 (1987).
- ⁷¹S. C. Farantos, J. M. Gómez Llorente, O. Hahn, and H. S. Taylor, *J. Chem. Phys.* **93**, 76 (1990).
- ⁷²M. Mladenovic and Z. Bacic, *J. Chem. Phys.* **93**, 3039 (1990).
- ⁷³T. J. Lee and A. P. Rendell, *Chem. Phys. Lett.* **177**, 491 (1991).
- ⁷⁴J. A. Bentley, J. M. Bowman, B. Gazdy, and C. E. Dateo, *Chem. Phys. Lett.* **198**, 563 (1992).
- ⁷⁵J. A. Bentley, C.-M. Huang, and R. E. Wyatt, *J. Chem. Phys.* **98**, 5207 (1993).
- ⁷⁶H. Tang, S. Jang, M. Zhao, and S. A. Rice, *J. Chem. Phys.* **101**, 8737 (1994).
- ⁷⁷D. Sugny, M. Joyeux, and E. L. Sibert, *J. Chem. Phys.* **113**, 7165 (2000).
- ⁷⁸J. H. Kiefer, P. S. Mudipalli, A. F. Wagner, and L. Harding, *J. Chem. Phys.* **105**, 8075 (1996).
- ⁷⁹T. M. Ticich, M. D. Likar, H. R. Dubal, L. J. Butler, and F. F. Crim, *J. Chem. Phys.* **87**, 5820 (1987).
- ⁸⁰C. R. Bucher and K. K. Lehmann, *Chem. Phys. Lett.* **294**, 173 (1998).
- ⁸¹K. K. Lehmann and R. Z. Martínez (unpublished).
- ⁸²R. J. Barnes, A. F. Gross, and A. Sinha, *J. Chem. Phys.* **106**, 1284 (1997).
- ⁸³Variational calculations carried out according to the procedure described in Ref. 102, using the Carter–Handy–Mills potential (Ref. 93) and the dipole moment function proposed by Botschwina (Ref. 103).
- ⁸⁴K. K. Lehmann and A. M. Smith, *J. Chem. Phys.* **93**, 6140 (1990).
- ⁸⁵D. Cerny, R. Bacis, G. Guelachvili, and F. Roux, *J. Mol. Spectrosc.* **73**, 154 (1978).
- ⁸⁶H. Ito, Y. Ozaki, K. Suzuki, T. Kondow, and K. Kuchitsu, *J. Mol. Spectrosc.* **127**, 283 (1988).
- ⁸⁷B. R. Rehfuß, M.-H. Suh, T. Miller, and V. E. Bondybey, *J. Mol. Spectrosc.* **151**, 437 (1992).
- ⁸⁸C. K. Luk and R. Bersohn, *J. Chem. Phys.* **58**, 2153 (1973).
- ⁸⁹M. Peric, H. Dohmann, S. D. Peyerimhoff, and R. J. Buenker, *Z. Phys. D: At., Mol. Clusters* **5**, 65 (1987).
- ⁹⁰For the same reasons mentioned above in the calculation of the photodissociation wavelengths, this is only an approximate value and constitutes an upper limit: Any transition departing from the ground vibrational state is going to occur, if it has a significant amplitude, at a relatively short bond length, thus requiring more energy to reach the ¹Π excited state than the value used in our calculations.
- ⁹¹Collisional relaxation studies are a good example: since the first vibrational excitation populates a single rotational state, a very short delay between the pump and jump pulses combined with a low sample pressure would result in vibrational spectra consisting of a single rotational line in every branch of the spectrum. As the delay is increased, collisional relaxation populates the other rotational states in (0,0,4) and more lines appear in the spectra. Although we observed these effects in our experiment, in this work we decided to focus our efforts in the spectroscopic part.
- ⁹²D. Romanini and K. K. Lehmann, *J. Chem. Phys.* **105**, 68 (1996).
- ⁹³S. Carter, I. M. Mills, and N. C. Handy, *J. Chem. Phys.* **99**, 4379 (1993).
- ⁹⁴S. Carter and N. C. Handy, *Comput. Phys. Rep.* **5**, 115 (1986).
- ⁹⁵S. Carter, I. M. Mills, and N. C. Handy, *J. Chem. Phys.* **97**, 1606 (1992).
- ⁹⁶S. Carter, N. C. Handy, and I. M. Mills, *Philos. Trans. R. Soc. London, Ser. A* **332**, 309 (1990).
- ⁹⁷J. M. Brown *et al.*, *J. Mol. Spectrosc.* **55**, 500 (1975).
- ⁹⁸G. P. Morley, I. R. Lambert, M. N. R. Ashfold, K. N. Rosser, and C. M. Western, *J. Chem. Phys.* **97**, 3157 (1992).
- ⁹⁹J. M. Pfeiffer, R. B. Metz, J. D. Thoemke, E. Woods, and F. F. Crim, *J. Chem. Phys.* **104**, 4490 (1996).
- ¹⁰⁰A. Callegari, P. Theule, J. S. Muentner, R. N. Tolchenov, N. Zobov, O. Polyanski, J. Tennyson, and T. R. Rizzo, *Science* **297**, 993 (2002).
- ¹⁰¹J. M. Bowman, S. Irle, K. Morokuma, and A. Wodtke, *J. Chem. Phys.* **114**, 7923 (2001).
- ¹⁰²A. M. Smith, W. Klempner, and K. K. Lehmann, *J. Chem. Phys.* **94**, 5040 (1991).
- ¹⁰³P. Botschwina, B. Schulz, M. Horn, and M. Matuschewski, *Chem. Phys.* **190**, 345 (1995), and private communication.